Geofísica Internacional (2026) **65-1**: 1935- 1950

Integrated Groundwater Potential and Quality Assessment in Pezu Dara Using Geophysical, GIS, and Hydrochemical Approaches

Luqman Khan[1], Sarfraz Khan[1]*, Muhammad Ali[1], Muhammad Akmal Sardar Ali[1] and Muhamad Kamal[1]

Abstract

Global climate change, increasing water demand, and rapid urbanization pose significant threats to groundwater sustainability in arid and semi-arid regions. Globally, approximately four billion people face water scarcity, with many developing countries, including Pakistan, struggling to ensure access to clean water. This study employs a comprehensive approach integrating surface and subsurface geophysical methods (electrical resistivity survey and borehole logs) with GIS-based Multi-Influencing Factor (MIF) analysis and hydrochemical assessment to evaluate groundwater potential and quality in the semi-arid Bannu Basin, Pezu Darra, Lakki Marwat District, northern Pakistan. Within a GIS framework, parameters such as slope, lineament density, drainage density, elevation, distance from rivers, topographic wetness index (TWI), land use/land cover, lithology, and rainfall were incorporated to assess groundwater potential. Additionally, 20 Vertical Electrical Sounding (VES) stations and borehole geophysical logs from two tube wells were analyzed to reveal the subsurface aquifer system and groundwater potential zones. Furthermore, nine water samples were analyzed for ten physicochemical parameters. The results indicate that 3.1% of the study area falls within a very low groundwater potential zone, while 11.83%, 63.81%, and 21.26% correspond to low, moderate, and high potential zones, respectively. In the western part of the study area, high-potential aquifers occur at depths of approximately 170 m, whereas in the eastern part, which represents a very low potential zone, aquifers occur at depths of about 235 m. Hydraulic properties of the layers overlying the aquifer were calculated from VES data to evaluate protective capacity. The longitudinal conductance ranges from 0.5 to 2.9 mhos, and the transverse resistance varies from 13,711 to 101,622 Ω·m², indicating heterogeneous aquifer protection. Overall, the findings demonstrate the effectiveness of integrating geospatial and geophysical techniques with hydrochemical analysis to provide a comprehensive understanding of groundwater potential and quality. These insights are crucial for sustainable water resource management, informed groundwater development, and climate-resilient planning in semi-arid regions.

Key words: Groundwater potential; Electrical resistivity survey; Multi-Influencing Factor analysis; Hydrochemical assessment; Sustainable water management.

Resumen

El cambio climático global, el aumento de la demanda de agua y la rápida urbanización representan graves amenazas para la sostenibilidad del agua subterránea en las regiones áridas y semiáridas. A nivel mundial, cerca de cuatro mil millones de personas sufren escasez de agua, y muchos países en desarrollo, incluido Pakistán, enfrentan dificultades para garantizar un acceso confiable al agua potable. Este estudio adopta un enfoque integral que combina métodos geofísicos de superficie y subsuperficie (sondeos eléctricos verticales y registros de perforación) con un análisis basado en SIG mediante el método de Factores Múltiples de Influencia (MIF) y una evaluación hidroquímica, con el fin de evaluar el potencial y la calidad del agua subterránea en la cuenca semiárida de Bannu, Pezu Darra, distrito de Lakki Marwat, norte de Pakistán. Dentro del marco SIG, se incorporaron parámetros como la pendiente, densidad de lineamientos, densidad de drenaje, elevación, distancia a los ríos, índice topográfico de humedad (TWI), uso/cobertura del suelo, litología y precipitación para delimitar las zonas de potencial de agua subterránea. Se analizaron veinte sondeos eléctricos verticales (VES) y registros geofísicos de dos pozos tubulares para caracterizar el sistema acuífero subterráneo. Además, se examinaron nueve muestras de agua para diez parámetros fisicoquímicos. Los resultados muestran que el 3,1% del área de estudio corresponde a una zona de potencial muy bajo, mientras que el 11.83%, 63.81% y 21.26% corresponden a zonas de potencial bajo, moderado y alto, respectivamente. En la parte occidental del área, los acuíferos de alto potencial se encuentran a profundidades de aproximadamente 170 m, mientras que en la parte oriental —clasificada como zona de potencial muy bajo— los acuíferos se localizan a profundidades cercanas a 235 m. Las propiedades hidráulicas de las capas suprayacentes se estimaron a partir de los datos VES para evaluar la capacidad de protección del acuífero. La conductancia longitudinal varía de 0,5 a 2,9 mhos, y la resistencia transversal oscila entre 13.711 y 101.622 Ω·m^2, lo que indica una protección heterogénea del acuífero. En conjunto, el estudio demuestra la eficacia de integrar análisis geoespaciales, geofísicos e hidroquímicos para desarrollar una comprensión integral del potencial y la calidad del agua subterránea. Estos resultados son fundamentales para la gestión sostenible de los recursos hídricos, el desarrollo informado de las aguas subterráneas y la planificación hídrica resiliente al clima en regiones semiáridas.

Palabras clave: Potencial de aguas subterráneas; Sondeo eléctrico vertical; Análisis de factores múltiples; Evaluación hidroquímica; Gestión sostenible del agua.

Received: July 9, 2025; Accepted: October 20, 2028; Published on-line: January 1, 2026.

Editorial responsibility: Dra. María Aurora Armienta Hernández

* Corresponding author:Sarfraz Khan, sarfraz_qau@yahoo.com
[1] National Centre of Excellence in Geology, University of Peshawar, Peshawar, 25130, KP, Pakistan

Luqman Khan, Sarfraz Khan, Muhammad Ali, Muhammad Akmal Sardar Ali and Muhamad Kamal
https://doi.org/10.22201/igeof.2954436xe.2026.65.1.1900

1. Introduction

Groundwater is a vital resource for drinking, agriculture, and industry, yet its sustainability is increasingly threatened by climate change, rapid urbanization, and over-extraction (Mechal *et al.*, 2015; Fentahun *et al.*, 2023). Persistent droughts and insufficient precipitation have intensified groundwater dependence in arid and semi-arid regions (Kumar, 2016). In addition, unregulated industrial activities and inadequate waste management allow contaminants to infiltrate aquifers, posing environmental and public health risks (Mathiazhagan *et al.*, 2015). Globally, more than four billion people face freshwater scarcity, and 26% lack access to safe drinking water (Fatta-Kassinos *et al.*, 2016; Bonazzi, 2023). Groundwater provides about 35% of the world's total water supply, underscoring the urgency of proper assessment and management (Akbar *et al.*, 2022).

In Pakistan (Figure 1), where agriculture dominates, per capita water availability has dropped from 5,000 m³ in 1947 to 1,000 m³, with projections indicating a further decline to 800 m³ by 2025 (Iqbal and Iqbal, 2015; Qureshi, 2017; Ahmad *et al.*, 2023). Currently, groundwater meets 90% of domestic needs and over 50% of agricultural demand (Lytton and Ahmed, 2022). Identifying groundwater potential zones is therefore essential for sustainable resource management (Subba Rao, 2006; Shao *et al.*, 2020).

Previous studies in the Bannu Basin have primarily focused on large-scale assessments without providing a detailed understanding of groundwater resources at the local level. For example, Suliman *et al.* (2021) applied the Analytical Hierarchy Process to identify potential recharge sites, Farid *et al.* (2017) used variogram modeling for electrical resistivity data to characterize hydrogeology, and Nazir *et al.* (2024) employed GIS-based Multi-Influencing Factor (MIF) analysis for groundwater potential mapping. However, these studies did not fully integrate geospatial, geophysical, and hydrochemical approaches to evaluate groundwater potential and quality comprehensively.

The present study addresses this gap by adopting a multi-method approach that combines satellite remote sensing, GIS-based MIF analysis, Vertical Electrical Sounding (VES), and hydrochemical assessments. This integration provides a detailed understanding of subsurface lithology, aquifer characteristics, and groundwater quality in Pezu Dara, Lakki Marwat District, Pakistan—an area facing growing water scarcity and agricultural dependency.

The main objectives of this study are: 1) To delineate groundwater potential zones using GIS-based Multi-Influencing Factor (MIF) analysis; 2) To characterize subsurface lithology and aquifer systems through Vertical Electrical Sounding (VES) and borehole data; 3) To assess groundwater quality using hydrochemical analysis; and 4) To integrate geospatial, geophysical, and hydrochemical findings for sustainable groundwater management strategies.

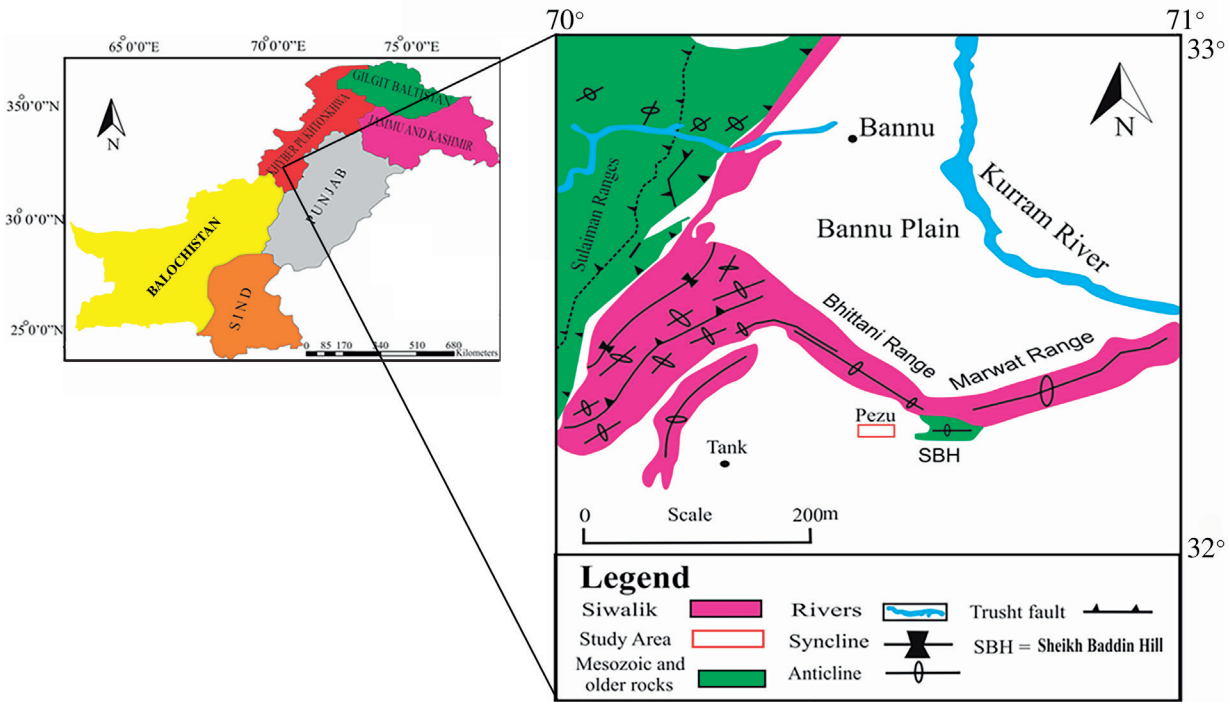

Figure 1. Geological map of the study area modified after Tariq *et al.* (2023).

2. Methodology

This study integrates geospatial and geophysical approaches to delineate groundwater potential zones. The MIF technique was employed to identify key groundwater determinants, Nasir *et al.* (2018), while Vertical Electrical Sounding (VES) was used for subsurface lithological modeling and aquifer system evaluation (Aizebeokhai and Oyebanjo, 2013; Babatunde *et al.*, 2018).

2.1 GIS and MIF Techniques

A weighted overlay analysis incorporating the MIF technique (Table 1) was applied to assess groundwater potential. Eleven key factors such as rainfall, slope, land use/land cover (LULC), distance from rivers, drainage density (DD), topographic wetness index (TWI), curvature, lineament density, and geology were selected based on literature review (Shahid *et al.*, 2000; Yeh *et al.*, 2009). These parameters were standardized by assigning scores and weights, as shown in Table 1 (Adham *et al.*, 2010; Magesh *et al.*, 2012; Rashid *et al.*, 2012). The weight for each influencing parameter was calculated using Equation 1 (Nasir *et al.*, 2018).

$$W_i = \frac{(A+B)}{\sum(A+B)*100} \quad (1)$$

where A and B represents major and minor influencing subclasses respectively. The thematic layers were then reclassified using ArcGIS 10.4, and the integrated layers were categorized into very high, high, good, and poor groundwater potential zones.

2.2 Geoelectrical measurements

A total of 20 VES points was acquired using the Schlumberger electrode configuration with a maximum current electrode spacing of 480m. Data collection was conducted using a SAS 4000 ABEM Terrameter and GPS (Raji and Abdulkadir, 2020). The direct current was injected into the ground through outer current electrodes (A and B) and the potential difference is measured between inner potential electrodes (M and N) (Telford *et al.*, 1990; Kearey *et al.*, 2002; Omosuyi *et al.*, 2007; El Makrini *et al.*, 2022). Using ohm's law electrical resistivity (ρ) is calculated as

$$\rho = K*(V/I) \quad (2)$$

$$K = \frac{\pi\left[\left(\frac{AB}{2}\right)^2 - \left(\frac{MN}{2}\right)^2\right]}{MN} \quad (3)$$

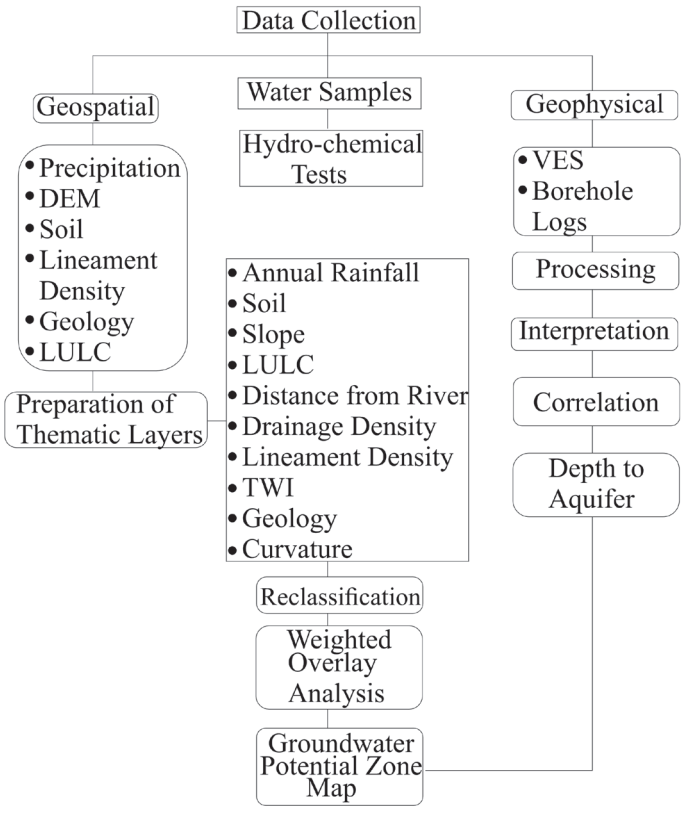

Figure 2. presents flowchart of adopted methodology.

Table 1. Proposed Summary Table for MIF Analysis

Parameter	Data Source	Class / Range	Influence on Groundwater	Weight (Wi)	Rank (Ri)
Slope	DEM (30 m)	0°–2°, 2°–5°, >5°	Low slope favors infiltration	0.25	1–3
Lineament Density	Remote sensing + GIS	High, Moderate, Low	Higher density = recharge	0.20	1–3
Drainage Density	Topographic maps	<2 km/km^2, 2–4 km/km^2, >4 km/km^2	Low density = high infiltration	0.15	1–3
Elevation	DEM	<300 m, 300–500 m, >500 m	Lower elevation = recharge	0.10	1–3
Distance from River	Satellite Imagery	<1 km, 1–3 km, >3 km	Closer proximity = recharge	0.10	1–3
TWI (Topographic Wetness Index)	DEM-based	High, Medium, Low	High TWI = higher moisture	0.05	1–3
Land Use / Land Cover (LULC)	Landsat imagery	Agriculture, Forest, Built-up, Barren	Agriculture enhances recharge	0.05	1–4
Lithology	Geological maps	Alluvium, Sandstone, Claystone	Alluvium > sandstone > clay	0.07	1–3
Rainfall	IMD / PMD Data	High (>500 mm), Moderate (250–500 mm), Low (<250 mm)	More rainfall = recharge	0.03	1–3

Notes:
Wi = Weight (calculated using MIF technique)
Ri = Rank (relative importance within each class)
Weights are proportional to the parameter's influence on groundwater potential
Classes and criteria follow previous studies (e.g., Subba Rao, 2006; Shao et al., 2020; Nazir et al., 2024)

where K is the geometric factor dependent on electrode arrangement. In heterogeneous subsurface conditions, the computed resistivity is termed apparent resistivity (Reynolds, 2011; Khalid *et al.*, 2019). Apparent resistivity data were further analyzed using Dar-Zarrouk parameters, including longitudinal conductance (S) and transverse resistance (T), calculated using equation 4 and 5 (Asfahani, 2013; Nwachukwu *et al.*, 2019; Opara *et al.*, 2021).

$$S = h/\rho_a = \sum_{i=1}^{n} \frac{h_i}{\rho_i} \quad (4)$$

$$T_R = h\rho_a = \sum_{i=1}^{n} (h_i \rho_i) \quad (5)$$

Where S is the longitudinal conductance, T_R is transverse resistance, h is thickness and ρ_a is the apparent resistivity.

The spatial distribution maps of resistivity along the study area at different depths were generated using ARC GIS.

2.2.1 Borehole Geophysics

Geophysical logs (Long Normal, Short Normal, Spontaneous Potential) and lithological logs from two boreholes were correlated with VES results to validate subsurface interpretations.

2.2.2 Hydro-chemical tests

Nine water samples from surface (water storage tanks) and subsurface sources (tube wells) were analyzed for electrical conductivity (EC), power of hydrogen (pH), Total Dissolved Solids (TDS), bicarbonate (HCO_3), chloride (Cl), sulfate (SO_4), nitrate (NO_3), calcium (Ca), magnesium (Mg), sodium (Na), and potassium (K). EC and pH were measured in situ (Table 2), while other parameters were analyzed in the laboratory following standard methods of Oguama *et al.* (2019) and Rasool *et al.* (2015).

3. Results

3.1 Geospatial Analysis

The Multi-Influencing Factor (MIF) analysis was performed by integrating ten thematic layers: lithology, elevation, slope, curvature, topographic wetness index (TWI), drainage density, lineament density, distance from river, land use/land cover (LULC), and rainfall. Each parameter was reclassified, weighted

Table 2. Presenting physiochemical parameters/units and adopted methodology.

Parameter/Units	Method	Parameter/Units	Method
Electrical Conductivity/ ds/m	EC-meter	pH	EC-meter
Sodium (mg/l)	Flame Photometer	Chloride (mg/l)	Titration
Potassium (mg/l)	Flame Photometer	Carbonate (mg/l)	Titration
Magnesium (mg/l)	Atomic absorption spectro-photometer	Bicarbonate (mg/l)	Titration
Calcium (mg/l)	Atomic absorption spectro-photometer	Sulfate (mg/l)	Titration

based on its relative influence on groundwater recharge, and combined using a weighted overlay technique in the GIS environment. (Table 1)

3.1.1 Elevation

Groundwater flow is influenced by elevation, generally moving from higher to lower regions (Thapa *et al.*, 2017). The elevation map (Figure 3a), derived from CARTOSAT-30 m DEM data in ArcGIS, shows that the study area ranges from 211 to 365 m. The lowest elevations (211–230 m) are in the south and southwest, while the highest (311–365 m) are in the east, with moderate elevations in the central region.

3.1.2 Geology

The availability and flow of groundwater of an area is influenced by the lithology by affecting infiltration, as well as the porosity and permeability of rock units, which determine their ability to store and transmit groundwater (Jhariya *et al.*, 2021). A field survey, supported by a comprehensive literature review and satellite data analysis, revealed that the study area is predominantly

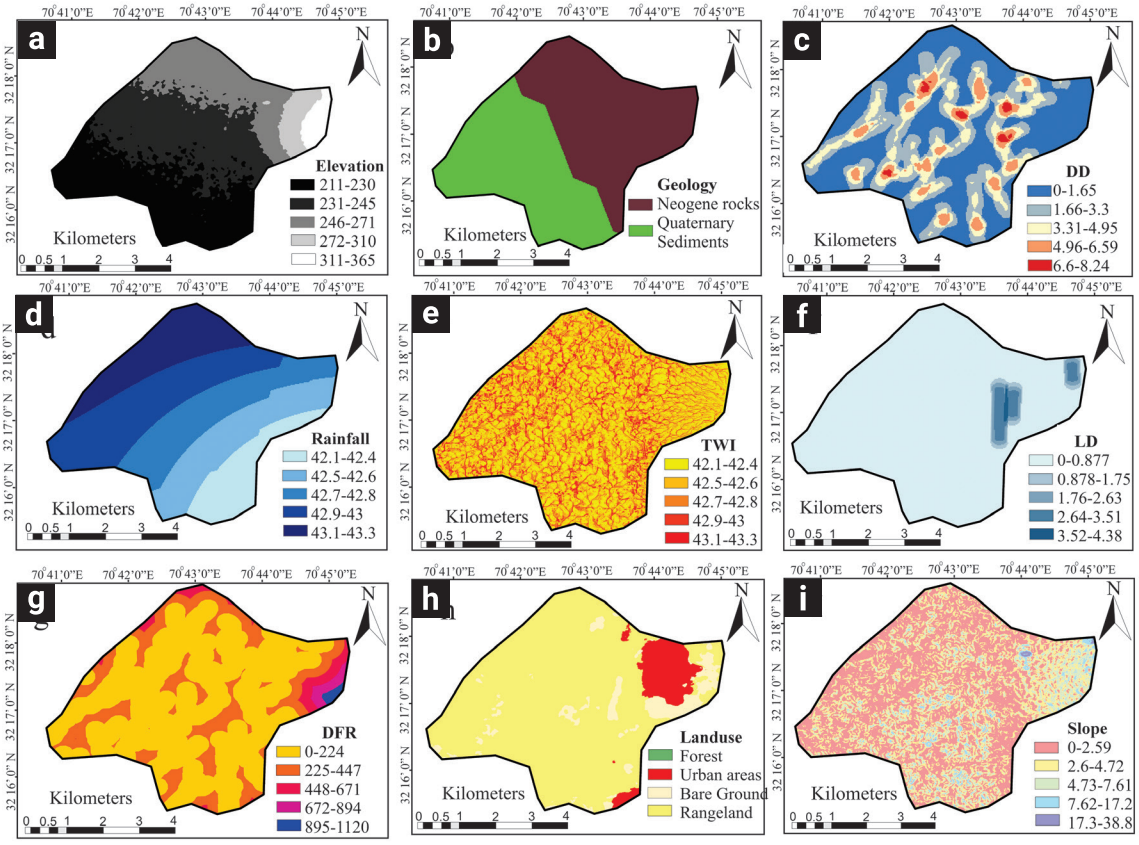

Figure 3. The Multi-Influencing Factor (MIF) analysis maps for ten thematic layers: lithology, elevation, slope, curvature, topographic wetness index (TWI), drainage density, lineament density, distance from river, land use/land cover (LULC), and rainfall.

composed of Quaternary sediments and Neogene sedimentary rocks (Figure 3b). The Quaternary sediments, part of the Siwalik group, consist of gravels, boulders, dirty sand, silt, and clay, and are found in the western and southwestern regions. The eastern and northern areas are mainly made up of Neogene sedimentary rocks, including sandstone, siltstone, claystone, and shale.

3.1.3 Drainage Density

Drainage density values range from 0 to 8.24 km/km^2 and is classified into five distinct categories (0-1.65, 1.66-3.3, 3.31-4.95, 4.96-6.59, 6.6-8.24 km/km2) as illustrated in Figure 3c. Low drainage density zones dominate the western and southwestern parts of the study area, whereas high drainage density is concentrated in the northern and eastern sectors

3.1.4 Rainfall

The spatial distribution of rainfall indicates minimal variation (Figure 3d), with values between 42.1 mm and 43.3 mm. Areas with relatively higher rainfall occur in the southwestern and central parts of the study area.

3.1.5 Topographic Wetness Index (TWI)

Topographic Wetness Index values range from 2.84 to 19.8 and was classified into five classes: very low (2.84-6.16), low (6.17-7.82), moderate (7.83-9.95), high (9.96-12.8), and very high (12.9-19.38) as shown in Figure 3e. Higher TWI zones are located in low-lying areas and valleys, while lower values occur in elevated and steeply sloping areas.

3.1.6 Lineament Density

Lineament density (km/km2) map generated from ASTER DEM (30m) shows density classifications: very low (0-0.877), low (0.878-1.75), medium (1.76-2.63), high (2.64-3.51), and very high (3.52-4.38) (Figure 3f). The highest density is concentrated along structural trends in the northern and northeastern parts, while the southwestern region exhibits sparse lineament development.

3.1.7 Distance from River

The distance from rivers was classified into five classes: very near (0–224 m), near (225–447 m), moderate (448–671 m), far (672–894 m), and very far (895–1120 m) (Figure 3g). Proximity to rivers decreases from north to south. The southern and southwestern regions are farther from major drainage channels, while the northern part is closer to perennial and seasonal streams.

3.1.8 Land use/Land cover

Land cover analysis indicates that rangelands and agricultural fields dominate the southwestern part of the study area (Figure 3h), while barren land and sparse vegetation cover the eastern and northeastern sectors.

3.1.9 Slope

Slope values range from 0° to 38.8°. Slopes are classified into five categories: flat (0–2.59%), gentle (2.6–4.72%), moderate (4.73–7.61%), moderately steep (7.62–17.2%), and steep (17.3–38.8%) (Figure 3i). Gentle slopes dominate the central and southwestern regions, while steep slopes are concentrated in the eastern highlands (Figure 3i).

3.1.10 Potential Groundwater Zone

Integration of thematic layers through weighted overlay analysis (WOA) produced a groundwater potential map. The groundwater potential map (Figure 4) shows that 3.10% of the area falls within the very low category, 11.83% in the low category, 63.81% in the moderate category, and 21.26% in the high category. High potential zones are primarily distributed in the southern and southwestern sectors, whereas very low potential zones occur in the eastern part.

3.2 Geophysical Analysis

3.2.1 Resistivity Data and VES Interpretation

After data acquisition the field curves were compared with standard curves and the true resistivity model was evaluated using partial curve matching. Final analysis was performed with the IPI2Win software using half of the current electrode separation (AB/2) on the x-axis and apparent resistivity values on the y-axis. Example graphs for VES 5, VES 11, VES 15 and VES 17 are shown in Figures 5a-d, where the red line indicates processed curves with minimum RMS error and the blue line represents the data processing outcome. The vertical and horizontal segments of the blue line show true resistivity and layer thickness.

Table 3 summarizes the interpreted VES survey revealing that the area is underlain by four to five geo-electric layers. The succession comprises coarse-grained sandstone, gravel, siltstone, sandy clay, and clay, as identified from outcrop observations, borehole cores, and geophysical logs. The coarse-grained sandstone and gravel units exhibit high resistivity values (typically 80–200 Ω·m), moderate to high porosity, and well-developed cross-bedding, indicating deposition under high-energy fluvial

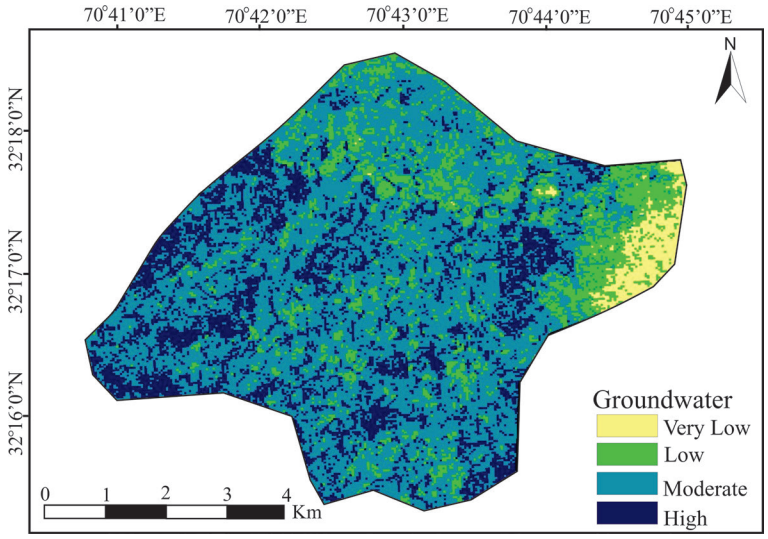

Figure 4. Represents the groundwater potential zones map of study area using weighted overlay analysis.

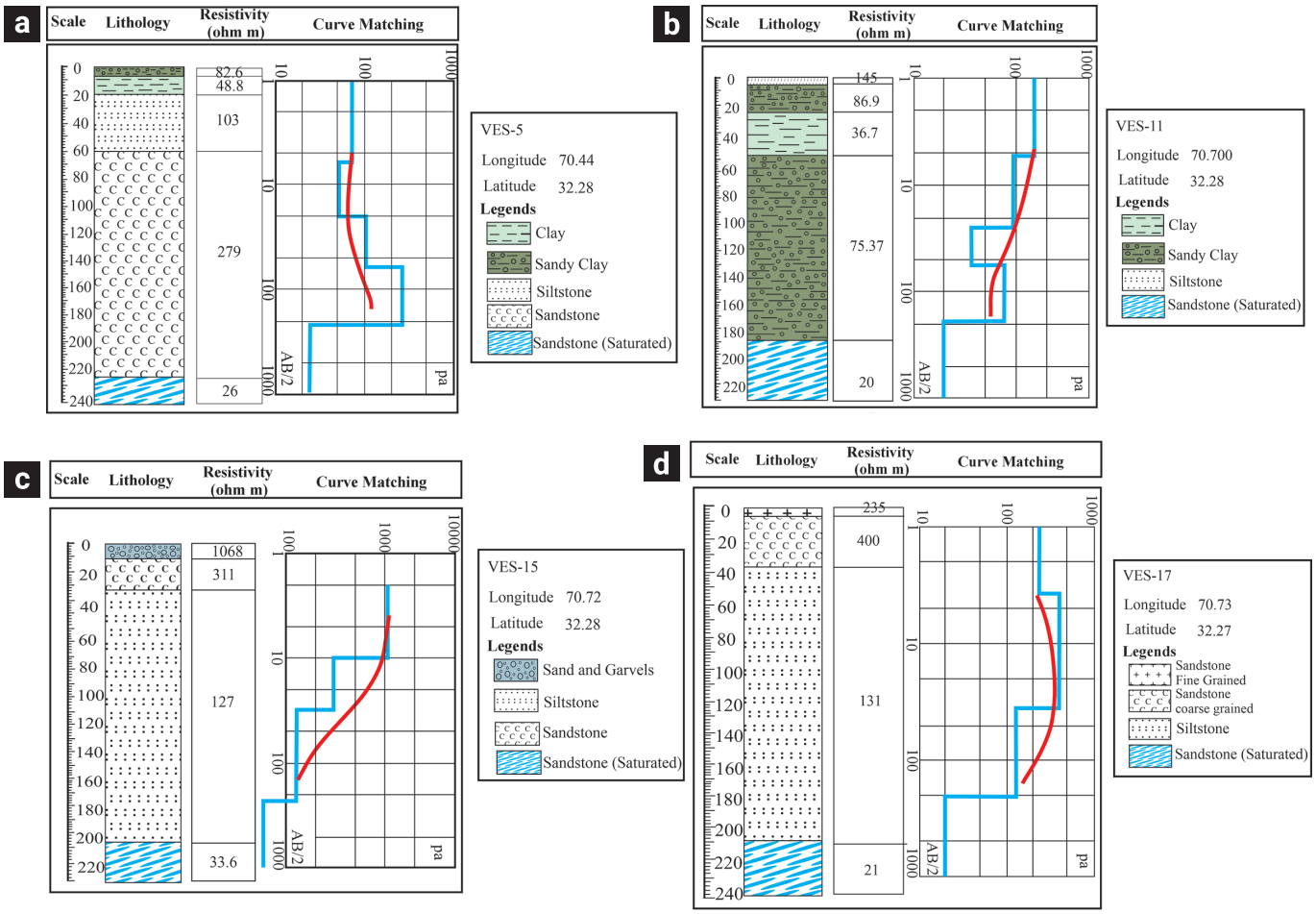

Figure 5a-d. showing vertical electrical sounding (VES) points 5, 11, 15 and 17 acquired at different locations across the study area. The resistivity models generated represents number of subsurface layers and interpreted lithologies with thickness.

Table 3. Representative results of interpreted layer parameters from the study area.

Station	Latitude	Longitude	Layer resistivity (ohm m)					Layer Thickness					Curve Type
VES			ρ1	ρ2	ρ3	ρ4	ρ5	h1	h2	h3	h4	h5	
1	32.27809043	70.73004102	239.8	79.7	342.4	116.5	23.28	5.9	12.54	19	166	∞	HQ
2	32.28585581	70.72925161	390	128	76.9	183	22.9	4.95	11.95	13.42	180	∞	HQ
3	32.29050109	70.72919769	239	59	380	126	23.3	2.8	22.5	32.3	158	∞	HH
4	32.29912472	70.73053333	125.3	81.2	366	86	23	3.6	31.8	33	150	∞	HH
5	32.28288069	70.74407833	82	48	103	269	26	5.92	16.8	44.2	158	∞	HH
6	32.2949737	70.7421838	241	42.3	347	25.1		9.76	59.2	163	∞		HH
7	32.28415373	70.71240867	122	71.9	147	388	32.6	6.44	12.5	15.4	153	∞	HK
8	32.29256083	70.71680971	657	146	52.7	227	31.3	4.37	17.7	23.8	164	∞	QK
9	32.30381356	70.71369828	1184	191	64.3	606	35	5.46	21	16.8	161	∞	QK
10	32.29376847	70.70335809	242	438	75	155	32.6	2.76	6	35	151	∞	KK
11	32.27911524	70.7001492	145	86.9	36.7	75.37	20	5.2	18.8	26	127	∞	QK
12	32.27228377	70.6833659	233.6	371	127.4	83.84	32.51	2	7	25.6	141	∞	KQ
13	32.28672427	70.6932722	77.62	396.4	45.24	120.6	38.77	1.73	8.87	14.5	145	∞	KK
14	32.27123705	70.69925818	516	239	32.5	185	22.7	5.4	7.3	15.7	152	∞	QK
15	32.28201941	70.72324238	1068	311	127	33.6		12.68	23	172	∞		QQ
16	32.26659036	70.71408891	1407	388	202	36		5.76	11	179	∞		QH
17	32.27048616	70.72464231	235	400	131	21		3.64	32	174	∞		KH
18	32.27603323	70.71665302	472	235	106.8	34		3.7	32	159	∞		QQ
19	32.25835819	70.70621009	1303	776	359	244	33	4.28	10	32.5	142	∞	QQ
20	32.25838378	70.72262199	564	885	279	179	34.7	2.5	5.3	33.8	139	∞	KQ

channel conditions. In contrast, siltstone and sandy clay layers show intermediate resistivity (20–50 Ω·m) and parallel to ripple laminations, characteristic of overbank and floodplain deposits. The clay horizons, with low resistivity (<10 Ω·m) and massive structure, suggest sedimentation in low-energy lacustrine or floodplain swamp environments. Collectively, these features support deposition within a mixed fluvial–lacustrine system (Table 4) (Jones *et al.* 2018).

The data revealed a variety of curve types (HH, HQ, QK, QQ, KK, KQ, HK, QH, KH), indicating heterogeneous resistivity and variability in layer properties due to erosion and sediment transport (Farid *et al.*, 2014).

3.2.2 Aquifer Characteristics (Dar Zarrouk Parameters)

The Dar-Zarrouk parameters derived from subsurface geo-electric layers overlying aquifer plays a crucial role in comprehending the spatial distribution of aquifer geometry and its protective capacity (Table 5) (Oli *et al.*, 2021; Utom *et al.*, 2012; Naidu *et al.*, 2021). Tube well lithological logs confirmed multiple stratigraphic units. Tube well No. 1 revealed gravels and boulders at the surface, followed by sand and gravel, coarse-grained sandstone, medium- to coarse-grained sandstone, and saturated sandstone layers at depths up to 180 m. Protective capacity analysis from VES data indicated longitudinal conductance values between 0.5 and 2.9 mhos and transverse resistance ranging from 13,711 to 101,622 Ωm^2 (Figure 6). These results suggest moderate to good aquifer protection in most parts of the study area.

3.2.3 Aquifer Depth

Depth to the water level depends upon the recharge and discharge of groundwater, based on the vertical electrical sounding data depth to the sandstone aquifer presented in Figure 7 reveal that the water level is shallower in the western and southern portions of the study area. Moderate in the north and central parts while the depth is gradually increasing towards the northeast and east. The maximum depth of 232 m is observed at VES 6 in the northeast while the minimum depth of 170 meters at VES 12 in the west.

3.2.4 Iso-Resistivity Maps

Iso-resistivity maps at different depths (5 m, 30 m, 100 m, 150 m, and 250 m) show variations in lithology, with coarse-grained sandstone and gravel dominating high-resistivity zones and clay-rich units in low-resistivity zones (Figure 8).

The resistivity distribution across the study area exhibits a pronounced spatial variation (Table 6), which, when integrated with borehole lithology, outcrop characteristics, and geomorphological context, allows for robust facies interpretation. High-resistivity values (800–1300 Ω·m), observed in the northern, central, and southern regions, are indicative of materials with low electrical conductivity, typically associated with coarse-grained, well-drained sediments. Resistivity alone cannot define depositional processes (Archie, 1942), but borehole logs from these sectors reveal thick sequences of coarse-grained sandstone and gravel, with sedimentary structures such as planar and trough

Table 4. Summary of Lithologies, Signatures, and Environment.

Lithology	Grain Size	Structures / Observations	Resistivity (Ω·m)	Depositional Environment
Coarse Sandstone and Gravel	Medium to Very Coarse	Cross-beds; high porosity	80–200	High-energy fluvial channel
Siltstone / Sandy Clay	Fine sand to silt	Parallel laminations; load casts	20–50	Overbank floodplain
Clay	Clay (<0.002 mm)	Massive; shrink-swelling cracks	<10	Lacustrine/floodplain swamp

Table 5. longitudinal conductance and protective capacity rating (modified after Olorunfemi *et al.*, 1999).

Longitudinal conductance (mhos)	Protective capacity rating
> 10	Excellent
5-10	Very good
0.7-4.9	Good
0.2-0.69	Moderate
0.1-0.19	Weak
< 0.1	Poor

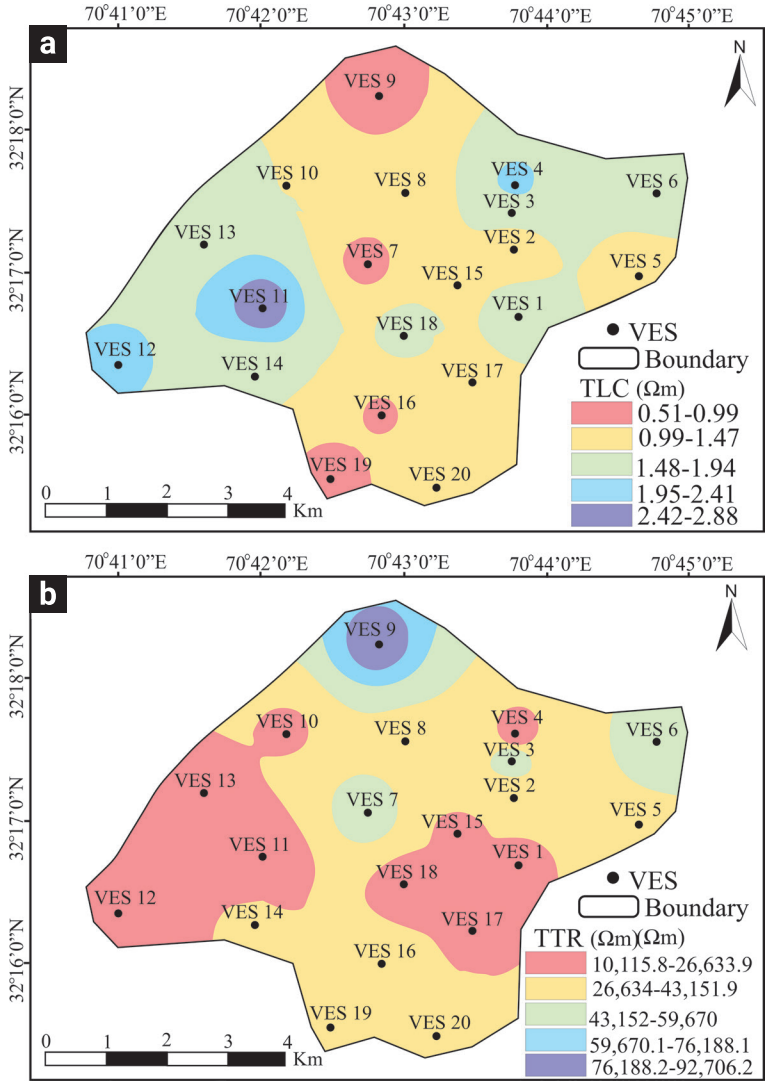

Figure 6. Showing a) total longitudinal conductance and b) total transverse resistance across the study area

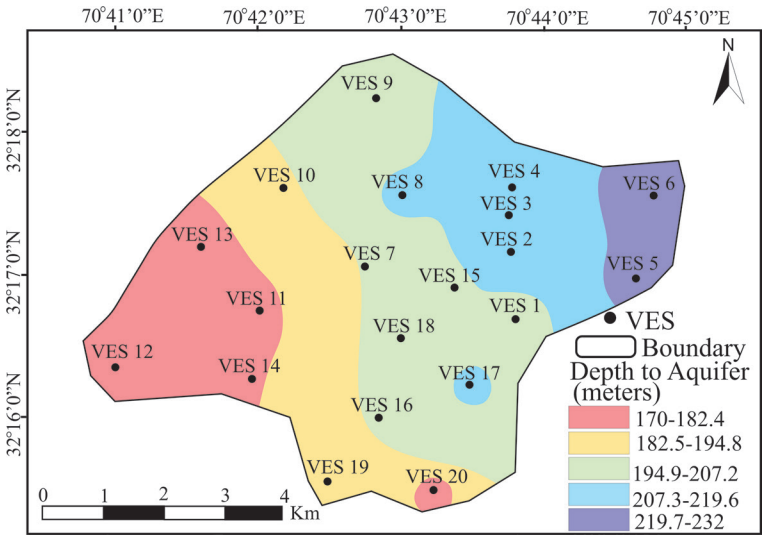

Figure 7. Showing depth to the Aquifer layer across study area.

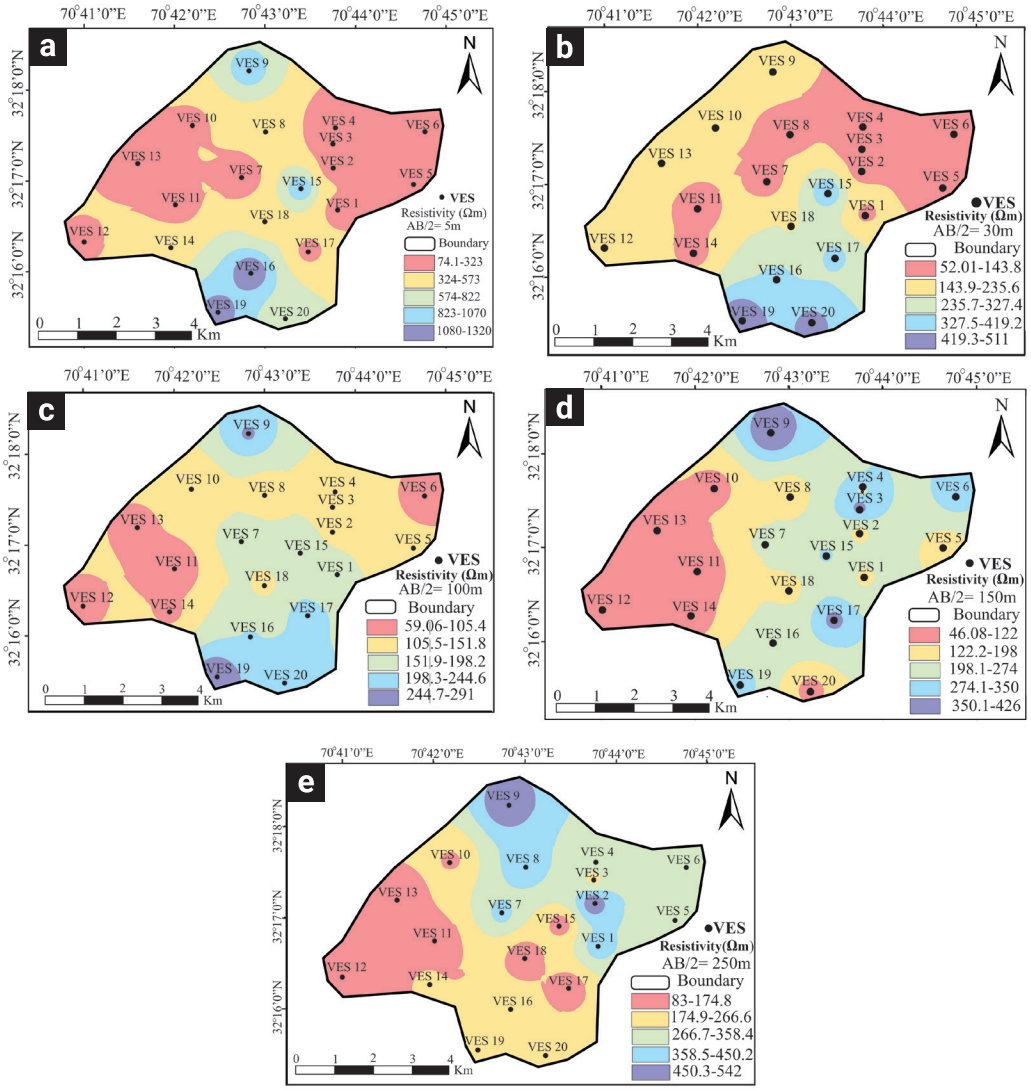

Figure 8. Showing resistivity distribution at different depths AB/2 a) 5m, b) 30m, c) 100m, d) 150m and e) 250m across the study area

Table 6. The resistivity distribution across the study area

Zone	Resistivity (Ω·m)	Supporting Evidence	Dominant Lithology	Depositional Environment
Northern, Central, Southern	800–1300	Borehole cores: coarse sand & gravel; Outcrop: cross-bedding	Coarse-grained sandstone, gravel	High-energy fluvial channels (braided/point bar)
Eastern, Western	50–300	Core: laminated silt & clay; Low-relief geomorphology	Silt, clay, fine sand	Low-energy lacustrine or floodplain lakes

cross-bedding, characteristic of high-energy fluvial systems (Miall, 1996; Bridge, 2003). Additionally, the geomorphic association with proximal alluvial fan and braided river systems further supports this interpretation.

In contrast, low-resistivity zones (50–300 Ω·m) occur in the eastern and western parts of the study area. Such values typically reflect fine-grained sediments (silt and clay) with higher clay content and greater water retention (Patel and Kumar, 2020). This interpretation is corroborated by core descriptions, which show laminated silts, massive clays, and occasional fine sand interbeds—features consistent with low-energy depositional settings, such as lacustrine basins and floodplain lakes. The lack of cross-stratification and the presence of horizontal lamination in these deposits indicate suspension settling under stagnant or slow-flow conditions (Bhattacharya, 2006).

These observations highlight that while geoelectrical resistivity provides a first-order proxy for lithology, it must be supplemented with core data, outcrop sedimentology, and geomorphological analysis for reliable paleoenvironmental reconstruction. The integration of these datasets allows differentiation between coarse-grained, channelized alluvial deposits and fine-grained lacustrine facies, which is crucial for understanding basin evolution and potential aquifer distribution.

3.2.5 Borehole Geophysics

Tube well No. 1 revealed five geological units: gravels and boulders, sand and gravel, coarse-grained sandstone, medium to coarse-grained sandstone, and saturated sandstone at 180 m depth (Figure 9). Tube well No. 2 showed similar units with more resistive and coarser formations (Figure 10). The lithologic units were interpreted primarily from geophysical well logs (gamma ray, resistivity, spontaneous potential) and drilling records. No continuous core was recovered; therefore, lithology and grain size estimates are inferred from log responses and driller's descriptions, which provide a first-order correlation framework. These interpretations should be considered tentative, pending core or outcrop confirmation

3.3 Hydrochemical Analysis

Nine groundwater samples were analyzed for ten physico-chemical parameters: pH, EC, TDS, Ca^{2+} , Mg^{2+}, Na^{+}, K^{+}, Cl^{-}, HCO_3^- , and SO_4^{2-} (Table 7).

3.3.1 Water Quality Parameters

- **pH:** It is ranged from 7.2 to 8.1 (within WHO permissible limits).
- **EC:** This parameter varied from 950 to 1850 µS/cm, indicating moderate mineralization.
- **TDS:** The TDS of all samples were below 1000 mg/L except two, which approached the permissible limit.

4. Discussion

4.1 Geophysical Interpretation and Limitations

The resistivity data reveal significant heterogeneity within the subsurface, with values ranging from 50–300 Ω·m in the eastern and western sectors to 800–1300 Ω·m in the northern, central, and southern sectors. High-resistivity zones (>800 Ω·m) are commonly associated with coarse-grained, well-drained sediments such as gravels and sandstones, whereas low-resistivity areas correspond to finer-grained sediments (silts and clays) with higher clay content and moisture retention (Patel & Kumar, 2020). However, it is important to emphasize that resistivity does not directly indicate depositional environment, as it is influenced by multiple factors including porosity, saturation, clay mineralogy, and salinity (Archie, 1942).

To reduce ambiguity, resistivity interpretations were cross-validated with well-log responses (gamma ray, spontaneous potential) and lithologic data from Tube Well No. 1, which indicates the presence of five major lithologic units: gravels and boulders, sand and gravel, coarse-grained sandstone, medium to coarse-grained sandstone, and a saturated sandstone layer at

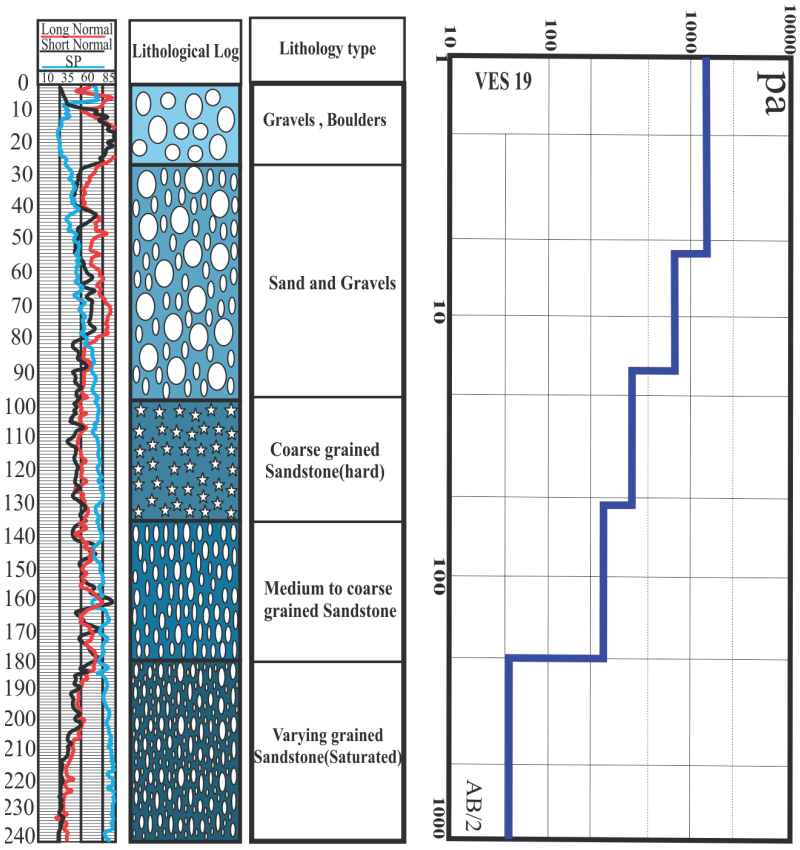

Figure 9. Showing geophysical logs (long normal, short normal, SP) response, lithological log and the result of nearby VES point.

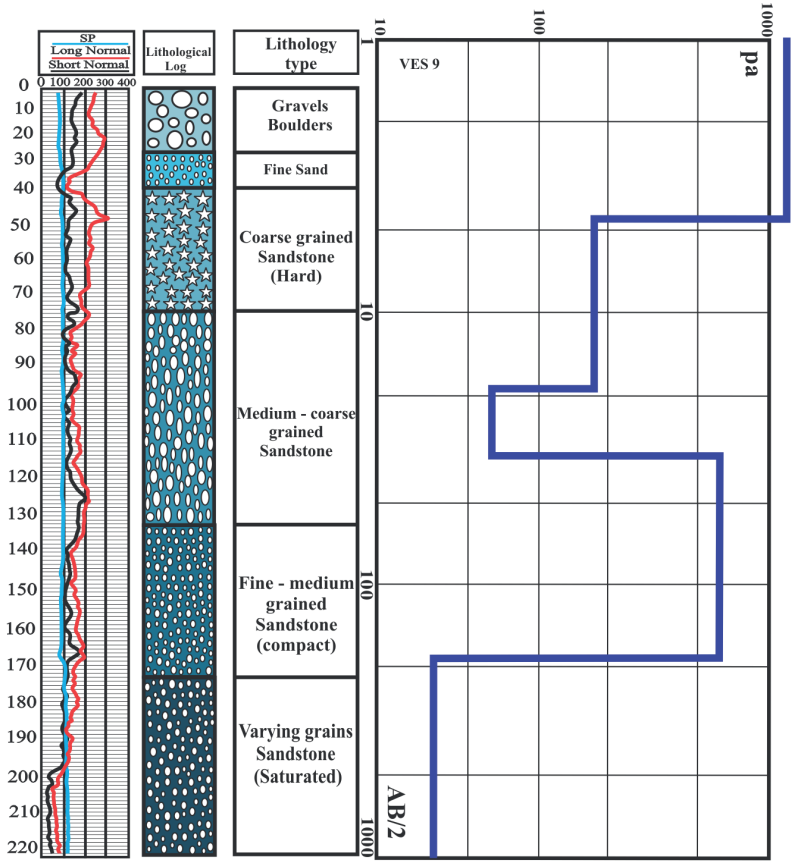

Figure 10. Showing the geophysical logs (long normal, short normal, SP) response and the result of nearby VES point

Table 7. Presenting hydrochemical analysis of surface and subsurface water samples taken across the study area.

Parameters	1	2	3	4	5	6	7	8	9	WHO Standard
pH	7.4	7.3	7.6	7.5	7.55	7.82	7.77	7.5	7.65	6.5-8.5
EC	245	382	297	278	305	343	316	267	362	400
TDS	680	702	743	905	796	880	774	695	820	500-1000
Cl	130	174	189	163	202	215	167	193	177	250
SO_4	184	215	164	223	198	230	212	240	228	250
Mg	27	33	26	42	38	31	46	34	28	50
Ca	66	55	70	48	62	72	59	71	56	75
K	8.3	7	9.1	10	6.9	8	9	7.3	8.8	12
HCO_3	425	340	380	422	295	476	412	326	478	500
Na	16	14	20	19	21	34	23	17	28	200

~180 m depth. While these observations strengthen the interpretation of channelized fluvial deposits in high-resistivity zones and fine-grained lacustrine facies in low-resistivity zones, the absence of continuous cores or outcrop tie points limits detailed facies characterization. Thus, the geophysical model provides a first-order proxy for lithologic distribution, requiring integration with sedimentological and geomorphic evidence for depositional environment reconstruction.

4.2 Geospatial Distribution and Depositional Framework

The geospatial distribution of resistivity zones aligns with the regional geomorphic framework. High-resistivity anomalies in the northern, central, and southern regions correspond to topographically higher areas associated with proximal alluvial fan and braided river systems, which are known to deposit coarse-grained sediments under high-energy conditions (Bridge, 2003; Miall, 1996). Conversely, low-resistivity zones in the eastern and western margins coincide with low-relief depressions, suggesting accommodation space for fine-grained lacustrine and floodplain deposits. Satellite imagery and digital elevation models reveal subtle paleochannel traces trending NW–SE across the central sector, supporting the interpretation of repeated channel avulsion and bar accretion processes.

This spatial facies distribution has important implications for groundwater potential and resource management. High-resistivity fluvial channels likely form productive aquifer zones where sand and gravel units exhibit sufficient thickness and lateral continuity, as indicated by Tube Well No. 1. In contrast, low-resistivity lacustrine deposits are expected to have lower hydraulic conductivity, potentially acting as aquitards or confining layers. These insights provide a preliminary hydrostratigraphic framework that can guide future drilling and groundwater exploration.

4.3 Uncertainties and Future Work

Despite the strong correlation between resistivity trends, geomorphic patterns, and borehole lithology, the interpretations presented here are subject to uncertainty due to the lack of continuous core data and sedimentary structure analysis. Future studies should incorporate core recovery, grain-size distribution, thin-section petrography, and additional geophysical methods (e.g., seismic, GPR) to refine depositional models. Moreover, integrating 3D geoelectrical inversion with GIS-based geomorphic analysis would enhance spatial resolution and improve facies prediction for groundwater exploration and basin evolution studies.

4.4 Implications for Water Resource Management

The integrated approach adopted in this study provides critical insights for sustainable groundwater management in semi-arid regions. Identification of high-potential zones in the southern and southwestern parts of the study area suggests that these areas should be prioritized for controlled groundwater development to meet domestic and agricultural demands. Moderate potential zones, which cover a significant portion of the study area, present opportunities for artificial recharge interventions such as check dams, percolation tanks, and recharge wells to enhance storage capacity and improve long-term sustainability.

The protective capacity analysis highlights the need for pollution control measures in low-protection areas to prevent aquifer contamination. Land-use planning should also restrict urbanization and industrial expansion in recharge zones to maintain natural infiltration. Furthermore, establishing a systematic groundwater monitoring framework—including periodic quality assessment and extraction limits—is essential to balance resource

utilization with recharge rates. These measures, combined with community awareness programs and policy-level interventions, can help ensure the resilience of groundwater resources under growing climate and population pressures.

5. Conclusion

This study demonstrates the effectiveness of integrating geospatial and geophysical methods, combined with hydrochemical assessment, for evaluating groundwater potential and quality in semi-arid regions. By incorporating multiple influencing factors through a GIS-based weighted overlay and validating results with VES surveys and borehole data, the research provides a comprehensive understanding of aquifer distribution, protective capacity, and water quality in the Pezu Dara region of Lakki Marwat District.

The analysis revealed that groundwater potential varies significantly across the study area, with the highest prospective zones concentrated in the southern and southwestern regions, while eastern areas exhibit limited potential and deeper aquifers. These spatial variations underscore the importance of adopting location-specific management strategies to ensure sustainable groundwater utilization.

Future work should focus on long-term monitoring of groundwater levels, numerical modeling to predict aquifer behavior under different extraction scenarios, and integration of climate change projections to assess future water availability. Additionally, advanced techniques such as remote sensing-based recharge estimation and isotopic tracing can further enhance the reliability of groundwater resource assessments.

6. Acknowledgements

The authors, thank the National Centre of Excellence in Geology (NCEG), University of Peshawar for its financial support. All authors thank the NCEG for permission to publish this work.

7. Declarations

The authors declare that they have no known competing financial interests or personal relationships that could have appeared to influence the work reported in this paper.

8. References

Adham, M., Jahan, C. S., Mazumder, Q., Hossain, M., & Haque, A.-M. (2010). Study on groundwater recharge potentiality of Barind Tract, Rajshahi District, Bangladesh using GIS and remote sensing technique. *Journal of the Geological Society of India, 75*, 432–438. doi: **https://doi.org/10.1007/s12594-010-0039-3**

Ahmad, S., Jia, H., Ashraf, A., Yin, D., Chen, Z., Xu, C., Chenyang, W., Jia, Q., Xiaoyue, Z., Israr, M., & Ahmed, R. (2023). Water resources and their management in Pakistan: A critical analysis on challenges and implications. *Water-Energy Nexus*, *6*, 137–150. doi: **https://doi.org/10.1016/j.wen.2023.10.001**

Aizebeokhai, A., & Oyebanjo, O. (2013). Application of vertical electrical soundings to characterize aquifer potential in Ota, Southwestern Nigeria. *International Journal of Physical Sciences, 8*(46), 2077–2085.

Akbar, H., Nilsalab, P., Silalertruksa, T., & Gheewala, S. H. (2022). Comprehensive review of groundwater scarcity, stress and sustainability index-based assessment. *Groundwater for Sustainable Development*, *18*, 100782. doi: **https://doi.org/10.1016/j.gsd.2022.100782**

Archie, G. E. (1942). The electrical resistivity log as an aid in determining some reservoir characteristics. *Transactions of the AIME*, 146(01), 54–62. doi: **https://doi.org/10.2118/942054-G**

Asfahani, J. (2013). Groundwater potential estimation using vertical electrical sounding measurements in the semi-arid Khanasser Valley region, Syria. *Hydrological Sciences Journal, 58*(2), 468 - 482. doi: **https://doi.org/10.1080/02626667.2012.751109**

Babatunde, A. A., Olubusola, I. S., & Emmanuel, O. F. (2018). Modeling of groundwater potential using Vertical Electrical Sounding (VES) and multi-criteria analysis at Omitogun Housing Estate, Akure, Southwestern Nigeria. *Asian Journal of Advanced Research and Reports*, 1(2), 1–11. doi: **https://doi.org/10.9734/ajarr/2018/v1i213043**

Bhattacharya, J. P. (2006). Deltas. From Environments to Facies Models. Elsevier.

Bonazzi, D. (2023). Imminent risk of a global water crisis, warns the UN World Water Development Report 2023. **https://www.unesco.org/en/articles/imminent-risk-global-water-crisis-warns-un-world-water-development-report-2023**

Bridge, J. S. (2003). *Rivers and Floodplains: Forms, Processes, and Sedimentary Record*. Wiley-Blackwell.

El Makrini, S., Boualoul, M., Mamouch, Y., El Makrini, H., Allaoui, A., Randazzo, G., & Muzirafuti, A. (2022). Vertical Electrical Sounding (VES) technique to map potential aquifers of the Guigou Plain (Middle Atlas, Morocco): Hydrogeological implications. *Applied Sciences, 12*(24), 12829. doi: **https://doi.org/10.3390/app122412829**

Farid, A., Khalid, P., Jadoon, K. Z., & Jouini, M. S. (2014). The depositional setting of the Late Quaternary sedimentary fill in southern Bannu basin, Northwest Himalayan fold and thrust belt, Pakistan. *Environmental Monitoring and Assessment, 186*, 6587–6604. doi: **https://doi.org/10.1007/s10661-014-3876-5**

Farid, A., Khalid, P., Jadoon, K. Z., Iqbal, M. A., & Shafique, M. (2017). Applications of variogram modeling to electrical resistivity data for the occurrence and distribution of saline groundwater in Domail Plain, north-

western Himalayan fold and thrust belt, Pakistan. *Journal of Mountain Science, 14*, 158–174. doi: **https://doi.org/10.1007/s11629-015-3754-9**

Fatta-Kassinos, D., Dionysiou, D. D., & Kümmerer, K. (Eds.). (2016). *Wastewater reuse and current challenges*. Springer. doi: **https://doi.org/10.1007/978-3-319-23892-0**

Fentahun, A., Mechal, A., & Karuppannan, S. (2023). Hydrochemistry and quality appraisal of groundwater in Birr River Catchment, Central Blue Nile River Basin, using multivariate techniques and water quality indices. *Environmental Monitoring and Assessment, 195*(6), 655. doi: **https://doi.org/10.1007/s10661-023-11198-6**

Iqbal, M. A., & Iqbal, A. (2015). A study on dwindling agricultural water availability in irrigated plains of Pakistan and drip irrigation as a future life line. *American-Eurasian Journal of Agricultural & Environmental Sciences, 15*(2), 184–190.

Jhariya, D. C., Khan, R., Mondal, K. C., Kumar, T., K., I., & Singh, V. K. (2021). Assessment of groundwater potential zone using GIS-based multi-influencing factor (MIF), multi-criteria decision analysis (MCDA) and electrical resistivity survey techniques in Raipur city, Chhattisgarh, India. *Journal of Water Supply: Research and Technology-Aqua*, *70*(3), 375–400. doi: **https://doi.org/10.2166/aqua.2021.129**

Johnson, H. M. (1962). A history of well logging. *Geophysics, 27*(4), 507–527.

Jones, R.T., Nguyen, H., & Smith, A.B. (2018). Resistivity contrasts in mixed fluvial–lacustrine systems. Journal of Applied Geophysics, 152, 50–62.

Kearey, P., Brooks, M., & Hill, I. (2002). *An introduction to geophysical exploration* (4th ed.). John Wiley & Sons.

Khalid, P., Sanaullah, M., Sardar, M. J., & Iman, S. (2019). Estimating active storage of groundwater quality zones in alluvial deposits of Faisalabad area, Rechna Doab, Pakistan. *Arabian Journal of Geosciences, 12*(6), 206. doi: **https://doi.org/10.1007/s12517-019-4372-6**

Kumar, C. (2016). Impact of climate change on groundwater resources. In Dinda, S. (Ed.) *Handbook of research on climate change impact on health and environmental sustainability* (pp. 196–221). IGI Global.

Lytton, L., & Ahmed, B. (2022). Managing groundwater resources in Pakistan's Indus Basin. *World Bank*. **https://www.worldbank.org/en/news/feature/2021/03/25/managing-groundwater-resources-in-pakistan-indus-basin**

Magesh, N. S., Chandrasekar, N., & Soundranayagam, J. P. (2012). Delineation of groundwater potential zones in Theni district, Tamil Nadu, using remote sensing, GIS and MIF techniques. *Geoscience Frontiers, 3*(2), 189–196. doi: **https://doi.org/10.1016/j.gsf.2011.10.007**

Mathiazhagan, M., Selvakumar, T., & Madhavi, G. (2015). Groundwater abstraction and contamination studies at Thiruvidanthai village, along East Coast Road in Chennai using electrical resistivity method with geochemical analysis. *Journal of Coastal Sciences, 2*(1), 12–18.

Mechal, A., Wagner, T., & Birk, S. (2015). Recharge variability and sensitivity to climate: The example of Gidabo River Basin, Main Ethiopian Rift. *Journal of Hydrology: Regional Studies, 4(B)*, 644–660. doi: **https://doi.org/10.1016/j.ejrh.2015.09.001**

Miall, A. D. (1996). The Geology of Fluvial Deposits. Springer. doi: **https://doi.org/10.1007/978-3-662-03237-4**

Naidu, S., Gupta, G., Shailaja, G., & Tahama, K. (2021). Spatial behavior of the Dar-Zarrouk parameters for exploration and differentiation of water bodies aquifers in parts of Konkan coast of Maharashtra, India. *Journal of Coastal Conservation, 25*, 1-9. doi: **https://doi.org/10.1007/s11852-021-00807-6**

Nasir, M. J., Khan, S., Zahid, H., & Khan, A. (2018). Delineation of groundwater potential zones using GIS and multi influence factor (MIF) techniques: a study of district Swat, Khyber Pakhtunkhwa, Pakistan. *Environmental Earth Sciences*, *77*(10), 367. doi: **https://doi.org/10.1007/s12665-018-7522-3**

Nazir, J., Ali, M., Sarwar, A., Khan, S., Rehman, K., Fahim, B., & Iqbal, B. (2024). Delineation and validation of GIS-based groundwater potential zones under arid to semi-arid environment using multi-influence-factors approach. *Geology, Ecology, and Landscapes,* 1-17. doi: **https://doi.org/10.1080/24749508.2024.2392382**

Nwachukwu, S., Bello, R., & Balogun, A. O. (2019). Evaluation of groundwater potentials of Orogun, South–South part of Nigeria using electrical resistivity method. *Applied Water Science, 9*(8), 184. doi: **https://doi.org/10.1007/s13201-019-1072-z**

Oguama, B. E., Ibuot, J. C., Obiora, D. N., & Aka, M. U. (2019). Geophysical investigation of groundwater potential, aquifer parameters, and vulnerability: A case study of Enugu State College of Education (Technical). *Modeling Earth Systems and Environment, 5*, 1123–1133. doi: **https://doi.org/10.1007/s40808-019-00595-x**

Oli, I., Ahairakwem, C., Opara, A., Ekwe, A., Osi-Okeke, I., Urom, O., Udeh, H., & Ezennubia, V. (2021). Hydrogeophysical assessment and protective capacity of groundwater resources in parts of Ezza and Ikwo areas, southeastern Nigeria. *International Journal of Energy and Water Resources, 5*, 57–72. doi: **https://doi.org/10.1007/s42108-020-00084-3**

Olorunfemi, M., Ojo, J., & Akintunde, O. M. (1999). Hydro-geophysical evaluation of the groundwater potentials of the Akure Metropolis, Southwestern Nigeria. 35, 207-228.

Omosuyi, G., Adeyemo, A., & Adegoke, A. (2007). Investigation of groundwater prospect using electromagnetic and geoelectric sounding at Afunbiowo, near Akure, Southwestern Nigeria. *Pacific Journal of Science and Technology, 8*(2), 172–182.

Opara, A., Eke, D., Onu, N., Ekwe, A., Akaolisa, C., Okoli, A., & Inyang, G. (2021). Geo-hydraulic evaluation of aquifers of the Upper Imo River Basin, Southeastern Nigeria using Dar-Zarrouk parameters. *International Journal of Energy and Water Resources, 5*, 259–275. doi: **https://doi.org/10.1007/s42108-020-00099-w**

Patel, S., & Kumar, P. (2020). Log interpretation of clay-rich floodplain deposits. Geophysics, 85(3), B273–B284.

Qureshi, W. A. (2017). Combating climate change in the Indus River Basin. *Kentucky Journal of Equine, Agriculture, & Natural Resources Law, 10*(1), 1-33.

Raji, W. O., & Abdulkadir, K. A. (2020). Geo-resistivity data set for groundwater aquifer exploration in the basement complex terrain of Nigeria, West Africa. *Data in Brief, 31*, 105975. doi: **https://doi.org/10.1016/j.dib.2020.105975**

Rashid, M., Lone, M. A., & Ahmed, S. (2012). Integrating geospatial and ground geophysical information as guidelines for groundwater potential zones in hard rock terrains of south India. *Environmental Monitoring and Assessment, 184*, 4829–4839. doi: **https://doi.org/10.1007/s10661-011-2305-2**

Rasool, A., Xiao, T., Baig, Z. T., Masood, S., Mostofa, K. M., & Iqbal, M. (2015). Co-occurrence of arsenic and fluoride in the groundwater of Punjab, Pakistan: Source discrimination and health risk assessment. *Environmental Science and Pollution Research, 22(24)*, 19729–19746. doi: **https://doi.org/10.1007/s11356-015-5159-2**

Reynolds, J. M. (2011). *An introduction to applied and environmental geophysics* (2a ed.). John Wiley & Sons.

Shahid, S., Nath, S., & Roy, J. (2000). Groundwater potential modelling in a soft rock area using a GIS. *International Journal of Remote Sensing, 21*(9), 1919–1924. doi: **https://doi.org/10.1080/014311600209823**

Shao, Z., Huq, M. E., Cai, B., Altan, O., Li, Y. (2020). Integrated remote sensing and GIS approach using Fuzzy-AHP to delineate and identify groundwater potential zones in semi-arid Shanxi Province, China. *Environmental Modelling & Software, 134*, 104868. doi: **https://doi.org/10.1016/j.envsoft.2020.104868**

Subba Rao, N. (2006). Groundwater potential index in a crystalline terrain using remote sensing data. *Environmental Geology, 50*, 1067–1076. doi: **https://doi.org/10.1007/s00254-006-0280-7**

Suliman, M., Samiullah, S., & Ali, M. (2021). Identification of Potential Groundwater Recharge Sites in a Semi-arid Region of Pakistan Using Saaty's Analytical Hierarchical Process (AHP). *Geomatics and Environmental Engineering*, 16, 53-70. doi: **https://doi.org/10.7494/geom.2022.16.1.53**

Tariq, M., Kashif, M., Ahmed, N., Ullah, Z., Mendez, J. N., & Miraj, M. A. F. (2023). Reservoir characteristics of Datta Formation (Early Jurassic), Marwat-Khisor Ranges, sub-Himalayas, Pakistan. *Petroleum Science, 20*(4), 2026–2044. doi: **https://doi.org/10.1016/j.petsci.2023.04.012**

Telford, W. M., Geldart, L. P., & Sheriff, R. E. (1990). *Applied geophysics*. Cambridge University Press.

Thapa, R., Gupta, S., Guin, S., & Kaur, H. (2017). Assessment of groundwater potential zones using multi-influencing factor (MIF) and GIS: A case study from Birbhum district, West Bengal. *Applied Water Science, 7*, 4117–4131. doi: **https://doi.org/10.1007/s13201-017-0571-z**

Utom, A., Benard, O., & Anthony, O. (2012). Estimation of Aquifer Transmissivity Using Dar Zarrouk Parameters Derived from Surface Resistivity Measurements: A Case History from Parts of Enugu Town (Nigeria). *Journal of Water Resource and Protection*, 4(12), 993-1000. doi: **https://doi.org/10.4236/jwarp.2012.412115**

Yeh, H.-F., Lee, C.-H., Hsu, K.-C., & Chang, P.-H. (2009). GIS for the assessment of the groundwater recharge potential zone. *Environmental geology,* 58, 185-195. doi: **https://doi.org/10.1007/s00254-008-1504-9**